Journal of Electroceramics 2:4, 215–228, 1998

Capacitive Type Gas Sensors

TATSUMI ISHIHARA[1*] & SHOGO MATSUBARA[2]

[1]*Department of Applied Chemistry, Faculty of Engineering, Oita University, Dannoharu 700, Oita 870-1192, Japan*
[2]*Material & Component Research Laboratory, Corporate Research Division, Kyushu Matsushita Electric Co., Ltd., Minoshima 4-1-62, Fukuaka, 812-8531 Japan*

Submitted October 10, 1997; Revised October 10, 1997; Accepted August 11, 1998

Abstract. Current status of capacitive type gas sensor were reviewed in this paper. Although the number of publications on capacitive type sensors has been limited so far, capacitive type sensors have good prospects given that the capacitor structure is so simple enabling miniaturization and achieving high reliability and low cost. Among the reported capacitive type sensors, detection of gas based on a change in dielectric layer thickness is most promising. On this point of view, capacitive type CO_2 and NO sensors using depletion layer formed at p-n junction of oxide semiconductor were introduced in detail. In addition, commercial capacitive type sensors for monitoring CO_2 based on this principle were mentioned. CO_2 concentration in office can be successfully monitored by the developed capacitive type CO_2 sensor.

Keywords: capacitive type sensors, CO_2, NO, humidity

1. Why Capacitive Type Sensor?

Detection of the concentration of a specific gas molecule in mixtures of various gas molecules is increasingly required for control and monitoring of various industrial or medical processes. In particular, there is a strong need for low cost and reliable solid state sensors. Great advances in chemical sensors for gas analysis have been made over the past 30 years. Table 1 summarizes the general characteristics of chemical sensors classified mainly by their detection mechanism. Oxide semiconductors, especially, SnO_2, have been widely studied for gas sensing and some have been put to practical use [1]. The principal advantages of oxide semiconductors are high stability and low cost, however, they lack selectivity. Although attempts have been made to promote selectivity in semiconductor-type sensors [2–6], the resulting selectivity is often inadequate. An advanced type of chemical sensor is the field effect transistor (FET) which provides for miniaturization and smart operation. Surface acoustic wave (SAW) sensors, to which the electronic technology is also applicable, are also being actively investigated. Solid electrolyte type sensor are inherently more selective and with the application of metal acid so-called ''auxiliary phase,'' it can expand the number of detectable gas species.

Little so far is known about the fundamentals of capacitive type chemical sensors, in particular, gas sensors based on capacitance change. However, capacitive-type sensors have good prospects given that the capacitor structure is so simple enabling miniaturization and achieving high reliability and low cost. In addition, amplification of capacitance is easily performed by oscillator circuits and thus, capacitive type sensors enable sensitive detection. In addition, oscillator circuits consist of only a standard resistor and sensor capacitor. Therefore, the signal treatment circuit is also very simple and low cost. Furthermore, the key advantage of the capacitive-type sensor is its selective detection of the specific gas molecules.

This paper reviews recent work on the capacitive type of sensor for selective gas detection with focus on the detection mechanisms. In particular, we examine a newly developed CO_2 sensor for monitoring indoor air quality.

* Correspondence author.

Table 1. Comparison of the sensing characteristics of various types of chemical sensors

	Semi-conductor	Catalytic combustion	Humidity	Solid electrolyte	Electro-chemical	Thermal conductive	Infrared absorption
Sensitivity	●	○	○	●	●	×	●
Accuracy	○	●	○	○	○	○	●
Selectivity	△	×	–	–	○	×	●
Response	●	○	△	●	△	○	○
Stability	●	○	○	○	×	○	○
Maintenance	●	○	○	●	×	○	△
Cost	●	●	●	○	○	○	△
Detectable concentration	few ppm	10 ppm	1–100 %r.h.	10^{-10}–1 atm	1–1000 ppm	1–100%	1 ppm–100%

●:excellent; ○:good; △:poor; ×:bad.

2. Principle Design for Capacitive Type Sensor

For detecting gases with a sensor, some quantity such as the resistivity or electromotive force (emf) of a device is measured as a function of the concentration of gas. In case of semiconducting gas sensors, charge transfer at the solid-gas interface by adsorption of gases is utilized. On the other hand, solid electrolytes sensors monitor the changes in chemical potential on the sensing electrode. Therefore, applying a so-called ''auxiliary phase'' which is in equilibrium with the object gas on the sensing electrode enables the detection of a gas which has no relationship with mobile ions in the solid electrolyte. It is reported that the auxiliary phase sometimes improves sensitivity to gases [7].

It is well-known that the capacitance is expressed as

$$C = \varepsilon_0 \varepsilon_r A/d$$

where ε_0, is the permittivity in vacuum, ε_r, the relative permittivity, A, the electrode area, and d the distance between electrodes, namely the thickness of the dielectric layer. For detection, the molecules of interest must induce a change in ε_r, A, or d. Except for the case of the humidity sensor, changes in electrode area are uncommon. While changes in dielectric constant due to the interaction between an immobilized antibody and antigen on electrode can be used to detect bio-molecules sensitively, it is generally unexpected for gas sensors given that the relative permittivity of most inorganic gases (except for H_2O) are similar. Therefore, changes in dielectric layer thickness are most promising for the detection of gases based on capacitance change. In the following, we summarize reports of capacitive type gas sensors based on this detection mechanism.

3. Capacitive Gas Sensor Based on Changes in Relative Permittivity

3.1. Capacitive Humidity Sensor

The humidity sensor is the most well-known capacitive type sensor. Since water has an abnormally large dielectric constant, changes in relative permittivity by the adsorption of water. provides a simple detection mechanism. In relation to other types of humidity sensors, the capacitive type has the advantage of high sensitivity over a wide humidity range [8–10]. The capacitive type sensor exhibits quick response, good reproducibility with no hysteresis, high selectivity and simple structure. Capacitive type humidity sensors can be divided into two groups of sensitive materials, i.e., polymer films and ceramics. Polymer films such as polyimides or cellulose acetates are generally used as the humidity sensitive dielectrics in these capacitive type humidity sensors. The relative permittivity of polymers such as polyimides are known to range from 3 to 6, whereas pure water has a far larger dielectric constant of 78.5 at 298 K. It follows that the capacitance of polymers changes sensitively with the adsorption of water. Studies on capacitive humidity sensor with porous ceramics also exist, albeit fewer in number.

A capacitive humidity sensor developed by Vaisala consists of a comb shaped Au electrode and a polymer electrolyte of cellulose acetate dissolved in ethylene dichloride as the humidity sensitive material. This

sensor is now widely used in radio-sonde and many other humidity-sensing instruments. As shown in Fig. 1, the capacitance-humidity characteristics show a near linear relation from 0 to 100% RH. This sensor has the advantages of good accuracy, low hysteresis (< 2% RH), and fast response time (90% response time achieved within 1 s). A microchip humidity sensor based on an insulated-gate field effect transistor was developed by Hijikigawa et al. [11,12]. A temperature sensing diode is fabricated on the same chip. The structure of this FET is shown schematically in Fig. 2. A hydroscopic polymer, cross-linked cellulose acetate butylate (CAB), whose electric capacitance changes with relative humidity, is used as the humidity sensing membrane. The output voltage V_{out} is given by the following equation.

$$V_{\text{out}} = V_o R_L g_m / (1 + C_i/C_s)$$

where V_o is the constant dc voltage driving the host IGFET, R_L the load resister connected with the drain electrode, g_m and C_i are the transconductance of the FET, and the capacitance of the gate insulator, respectively. Figure 3 shows the typical output voltage of the FET humidity sensor operating at 298 K. This micro sensor responds over the whole humidity range with a near linear relationship. The accuracy of this sensor, which is limited by the hysteresis of the membrane, is better than 3% RH. Furthermore, the response and recovery times are less than 30 s. It has good stability at room temperature and is durable in high humidity. A similar integrated relative humidity sensor, combining capacitive sensor with CMOS measurement circuit on the same silicon chip was developed by Silverthorne et al. [13]. The

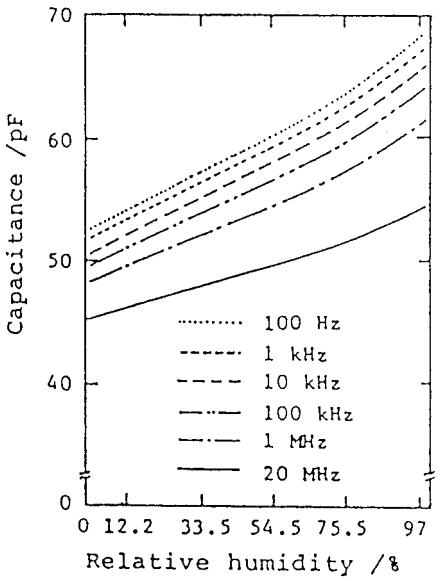

Fig. 1. Frequency dependence of the capacitance-humidity characteristics of the ''Humicape.''

dc voltage output agrees closely with theoretical values and varies linearly with relative humidity over the entire range from 0 to 100%. The response time was about 10 s, and hysteresis was within 1.6% of full scale output.

Capacitive humidity sensors based on ceramics have also been investigated. Alumina films, prepared by reactive ion plating, anodic oxidation, or vapor deposition, are known to be sensitive to humidity in both capacitive and resistive modes [14–17]. The capacitance of the porous alumina film increases with an increase in relative humidity due to the large relative permittivity of the adsorbed water. Control of

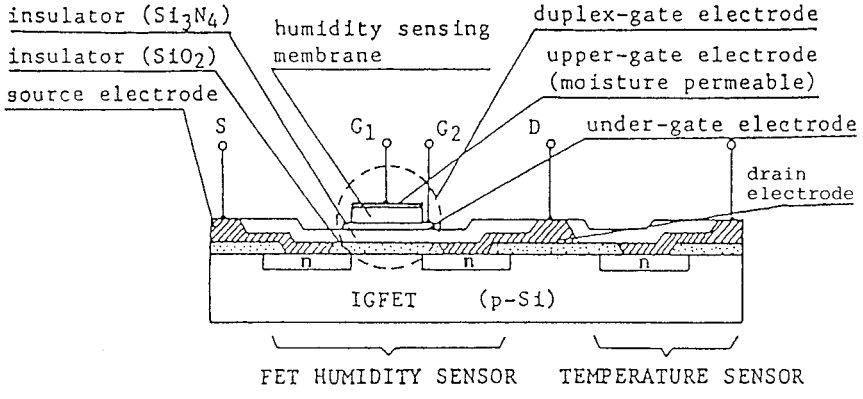

Fig. 2. Schematic cross-section of FET humidity sensor.

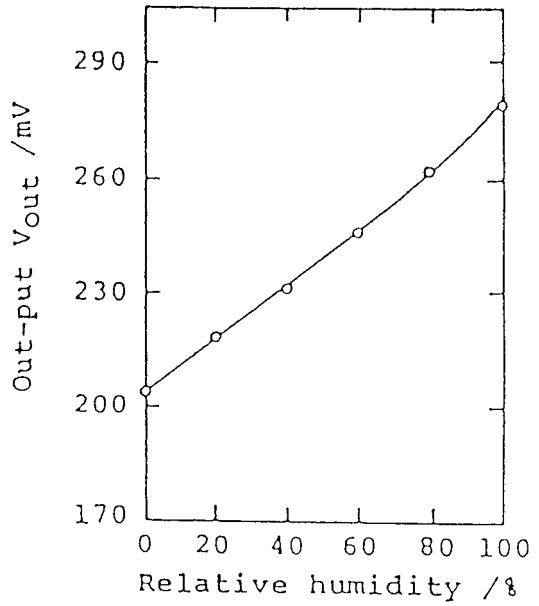

Fig. 3. Output response curve of FET type humidity sensor.

the microstructure of the film is of importance to insure good sensing characteristics as details for reactive ion plating [18] and anodic oxidation [19]. Furthermore, it was found necessary to leave the upper electrode thin and porous for rapid response.

Figure 4 shows a cross-section of a 1 mm^2 humidity-sensitive MOS capacitor [19]. A porous, thin alumina layer was prepared by anodizing the 1 mm thick aluminum evaporated on silicon dioxide. The porous upper electrode of gold was defined by a photolithographic technique. The humidity sensitive MOS capacitor can be incorporated into the gate of a

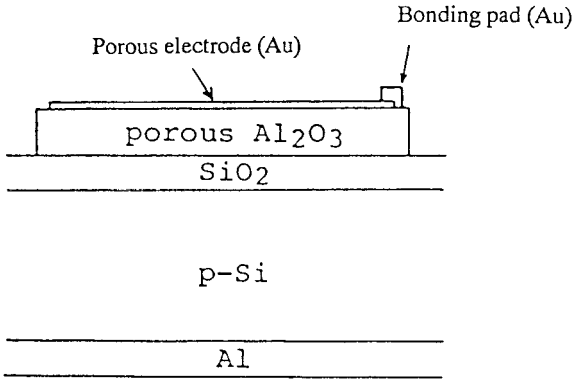

Fig. 4. Schematic cross-section of a humidity-sensitive MOS capacitor.

MOSFET in which the humidity can be detected from variations in the drain current.

In summary, the capacitive sensor has many advantages for humidity detection, i.e., small size, rapid response, low cost, and operation over wide humidity ranges [20,21]. In particular, the structure of the capacitive sensor is simple, and thus is easily fabricated on silicon chips by IC processing technology. The combination of a capacitive humidity sensor with CMOS measurement circuitry on a single silicon chip enables the development of a new intelligent sensor. Recent studies are focused on the development of polymers for the dielectric layer, since they provide the required stability in humidity as well as low hysteresis for adsorption and desorption of humidity.

3.2. Capacitive Type CO and Hydrocarbon Sensor

Recently, thin film of aluminophosphate(AlPO)-5 molecular sieve was used as the dielectric phase in a capacitance type chemical sensor for CO and CO_2 [22]. AlPO-n is a family of phosphorous molecular sieves which have ordered molecular sized pores. The AlPO-5 structure used for the dielectric layer consists of four- and six-membered rings of alternating phosphate and aluminum ions bridged by oxygen. These rings are arranged to produce one-dimensional channels 0.73 nm in diameter. The properties of AlPO-n are reviewed in detail [23] and one of the attractive properties of these materials is their heat stability. The molecular sized pore and acidity enable the unique adsorption property based on its size. In addition, it is expected that the adsorption of an analyte molecule affects a significant change in the molecular sieve dielectric property.

Figure 5 shows the schematic view of the AlPO-5 molecular sieve based sensor. TiN on silicon serves as the bottom electrode and the Au/Pd alloy patterned on top of the molecular sieve serves as the top electrode. The molecular sieve films were deposited onto the TiN by pulsed laser deposition or laser ablation followed by a hydrothermal treatment. Rutherford back scattering depth profile analysis suggests that the thickness of the ablated AlPO-5 film is 36 nm. The XRD measurement of films after deposition and hydrothermal treatment clearly indicates the presence of crystalline AlPO-5, corresponding to an estimated 19% degree of crystallinity relative to the target material. Figure 6 shows the plot of capacitance

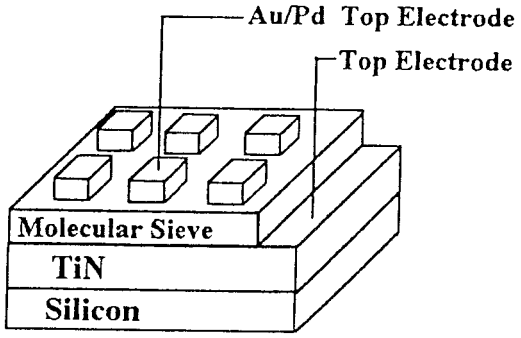

Fig. 5. Schematic view of the developed A1PO-5 molecular sieve based sensor.

versus thickness of the deposited AlPO-5 film at a potential of $+0.3$ V. The capacitance depends on the kind of gas, and differences in capacitance in good agreement with the sensitivity, become more significant with decreasing thickness of film. Although the mechanism for capacitance change is not clearly explained, it is speculated that CO or CO_2 strongly interact with AlPO-5 resulting in changes in the dielectric constant of AlPO-5. The thinnest films provide the greatest capacitance change, however, the leakage current also increases with decreasing thickness with a thickness of 200 to 300 nm being preferred. While the sensor responds reproducibly to H_2O, CO_2, and CO, the sensitivity to CO or CO_2 is far larger. The average capacitance ratios of 100% CO_2 to N_2 and 100% CO to N_2 with this sensor are 20 and 85, respectively.

On a similar sensing approach, zeolite was selected as the dielectric layer of a hydrocarbon sensing. Hydrocarbon adsorption influences the dielectric constant of zeolite [24]. Planar interdigital capacitors consisting of a thin film of H or Pt ion-exchanged Y type zeolite were studied as capacitive type sensors for hydrocarbons such as butane. The capacitance increased upon exposure to hydrocarbon varying from 20 to 120 s to attain equilibrium. The response time was reported to depend on the thickness of the zeolite layer and the operating temperature. Although the response time became short, the capacitance change decreased with increasing operating temperature. In particular, 323 K was desirable for operation, since the capacitance change became small and unstable above 373 K. Pt-Y coated devices showed larger sensitivity as compared to HY-zeolite.

Although the sensor sensitivity based on molecular sieves is rather low, it demonstrates that bipolar interactions between adsorbates and molecular sieves are of potential use in capacitive type gas sensors.

3.3. *Capacitive Type CO_2 Sensor*

Capacitive type CO_2 sensors based on changes in the dielectric properties of organically modified silicates have been reported [25]. Figure 7 shows the cross section and schematic view of the sensor. The sensitive layer consists of 3-amino-propyl-trimethoxysilane and propyl-trimethoxysilane and is fabricated on an integrated heater on a quartz-glass substrate. The capacitance of the sensitive layer was measured with an interdigital NiCr/Au electrode put under the

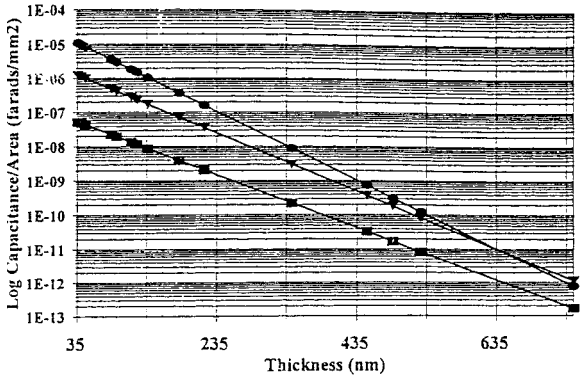

Fig. 6. Plot of capacitance versus thickness of the deposited A1PO-5 film.

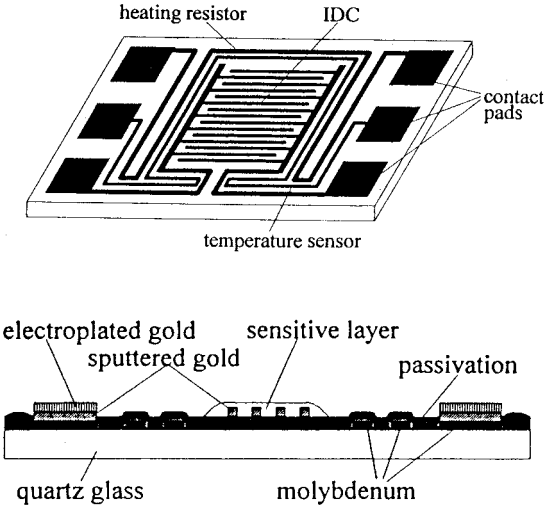

Fig. 7. Cross section and schematic view of the sensor based on organically modified silicate.

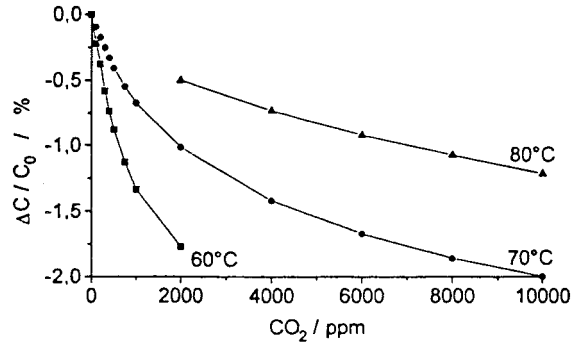

Fig. 8. Capacitance of the sensor as a function of CO_2 concentration.

film. The heating resister and temperature sensor were also fabricated on the same substrate. The sensor was operated at temperatures of 333–353 K. Under exposure to CO_2, the capacitance of the sensor decreases as shown in Fig. 8. The capacitance at 0 ppm CO_2 increases with temperature and the sensitivity decreases monotonically with increasing CO_2 concentration. Although the mechanism has not been discussed, it seems likely that the dielectric properties of the organic sensitive layer are reduced by the CO_2 adsorption. This sensor has an advantage of low temperature operation, however, interference by humidity is anticipated.

4. Capacitive Type Sensor Based on Thickness of Dielectric Layer

Capacitive type sensors based on changes in dielectric layer thickness are more attractive than those based on changes in the dielectric constant. There are two design approach for sensor development. In the first, the thickness of the dielectric layer actually changes in proportion to the concentration of the target molecules. Capacitive type bio-sensors are generally based on the actual changes in thickness of immobilized enzyme as the dielectric layer [26–28], for example, α-fenoprotein is detected by use of a monoclonal anti-α-fenoprotein film as the dielectric layer [26]. Capacitance decreases with increasing α-fenoprotein concentration, since the thickness of the anti-α-fenoprotein film increases due to antigen-antibody interactions. However, it is anticipated that the sensitivity gradually decreases or disappears by repeated exposure to the target molecules. In addition, these devices are characterized by a long period to response and/or recovery times. The second approach relies on the formation of depletion layers as the dielectric layer of the capacitor. Depletion layers formed between p and n type semiconductors, metal-oxide-semiconductors, or metal-semiconductor contacts are investigated for this purpose. Here, the electronic interactions between the target molecules and the interface change the carrier density in the semiconductor resulting in changes of the thickness of the depletion layer. Consequently, quick and reproducible responses are expected for these type of sensors.

4.1. Capacitive Type Sensor Based on the MOS Structure

Capacitive type sensors for hydrogen [29], ammonia [30], and humidity [31] were reported based on the use of the metal-oxide-semiconductor (MOS) structure. These MOS capacitive type sensors are based on changes in the depletion layer caused by changes in work function of the metal on exposure to the gas. The capacitance of MOS capacitors decrease with increasing bias as shown in Fig. 9 [30]. The adsorption of gas, for example, NH_3 shifts the capacitance-potential characteristics to the left. This can be understood by noting that the adsorbed gas changes the work function of the metal gate electrode which

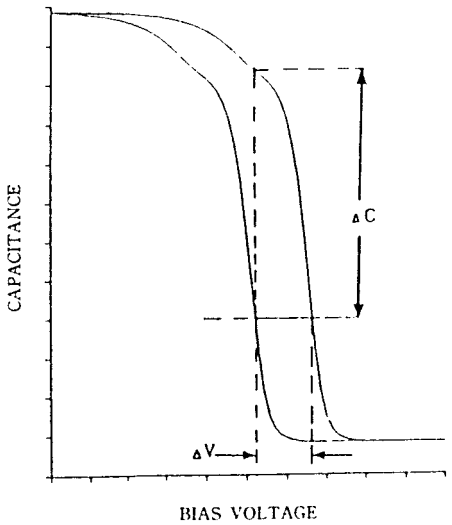

Fig. 9. Influence of NH_3 on capacitance-bias potential characteristics of MOS capacitor.

causes a change in the thickness of the depletion layer. Consequently, the dependence of the capacitance on bias potential is shifted by the adsorption of gas.

MOS capacitors were also studied for hydrogen sensing and it was reported that hydrogen was detected from the voltage change in capacitance-voltage curve of MOS capacitor consisting of palladium/SiO_2/p-Si [29] as shown in Fig. 10. The output voltages agreed well with the theoretically estimated ones. In addition, stable and reproducible responses were sustained over one month. On the other hand, it is also reported that the MOS capacitor which was applied on ZnO or SnO_2 added with Pt or Ag for the gate electrode is sensitive to O_2 and CO [32]. These MOS capacitive type sensors have an advantage of operating temperature lower than 373 K.

4.2. Capacitive Type CO_2 and NO_X Sensor Based on p-n Junction

The detection and control of CO_2 is of importance for various industrial and biological processes. Various systems have been proposed recently for CO_2 sensing from the viewpoint of reducing cost, miniaturization, and/or simplification of the detection system [33–36]. Since the reactivity of carbon dioxide is weak, output signals from CO_2 sensors are generally small, making selectivity an important target in the development of CO_2 sensors. While most CO_2 sensors reported so far are based on a solid electrolyte gas concentration cell [37–41], capacitive type sensors based on depletion layer control at p-n junctions formed in oxide semiconductor powders have recently been reported [42–44].

A mechanical mixture of $BaTiO_3$ and other metal oxides as dielectrics sandwiched between two parallel Ag electrode were used in the development of capacitive CO_2 sensors [45]. The changes in capacitance of $BaTiO_3$, PbO, and their equimolar mixture on exposure to 2% CO_2 are shown in Fig. 11. The sensitivity to CO_2 is expressed by the ratio of the capacitance in the sample gas to that in air in Fig. 11. The introduction of 2% CO_2 does not change the capacitance of $BaTiO_3$, while it slightly decreases that of PbO. On the other hand, the capacitance of the equimolar mixture of PbO and $BaTiO_3$ decreases significantly on exposure to 2% CO_2. The enhancement of CO_2 sensitivity results from the resemblance of the mixed oxide capacitor to the barrier-layer capacitor, and it is expected that the small changes in capacitance of PbO is amplified by mixing with $BaTiO_3$. The effects of mixing other oxides with $BaTiO_3$ on the CO_2 sensing characteristics are summarized in Table 2. The sensing characteristics depend strongly on the kinds of metal oxides used

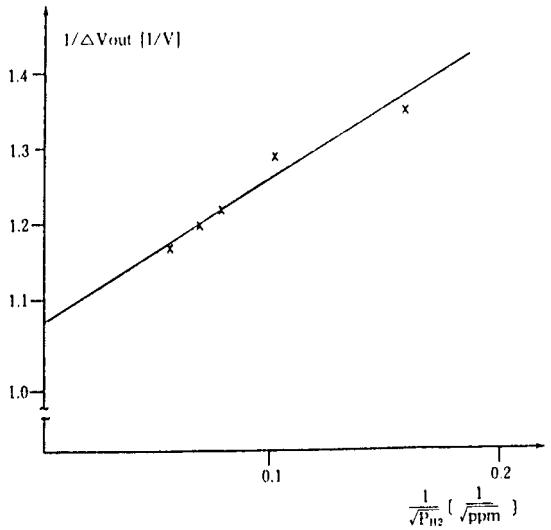

Fig. 10. Output voltages of MOS capacitor which consists of Pd/SiO_2/p-Si as a function of H_2 concentration.

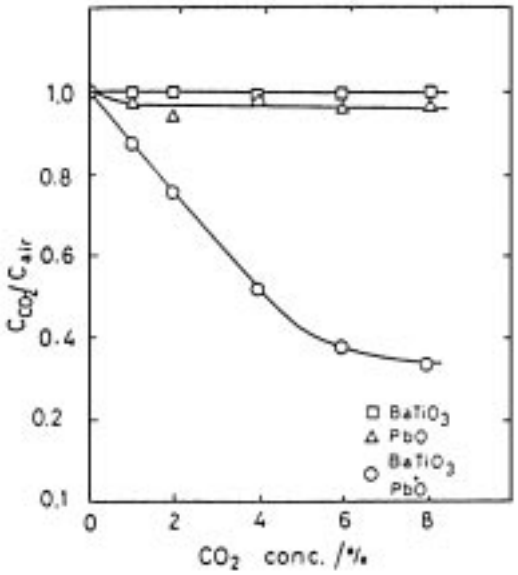

Fig. 11. Sensitivity to PbO, $BaTiO_3$, and equimolar mixtures related to carbon dioxide concentration.

Table 2. CO_2 sensing characteristics of the mixed oxide capacitor

Oxide	Operation temperature[1]/K	Sensitivity[2] c_{CO2}/c_{air}	Upper limit[3] of detection/%
CaO	>1173[4]	0.891	8
MgO	1140	0.329	10
La_2O_3	1039	0.451	8
Nd_2O_3	823	0.641	6
Y_2O_3	1032	0.794	10
CeO_2	934	0.410	8
PbO	774	0.711	6
NiO	828	0.441	20
CuO	729	2.892	6
ZrO_2	915	0.740	10
Co_3O_4[5]	801	0.362	6
Fe_2O_3	614	0.678	2
Bi_2O_3	718	0.824	2
V_2O_5	—	1.000	0
Nb_2O_5	—	1.000	0
SiO_2	—	1.000	0
Al_2O_3	—	1.000	0
SnO_2	—	1.000	0

[1] optimum temperature for CO_2 detection.
[2] sensitivity to 2% CO_2.
[3] A linear relationship between sensitivity and CO_2 concentration exists below this concentration.
[4] Higher than 1173 K.
[5] $BaTiO_3$:Co_3O_4 = 3:1.

[46]. Oxide capacitors containing basic oxides such as CaO, MgO, and La_2O_3 are sensitive to CO_2, but generally require high operating temperatures. On the other hand, the mixed oxides, NiO-$BaTiO_3$, CuO-$BaTiO_3$, and Co_3O_4-$BaTiO_3$ exhibit high sensitivity with optimum operating temperatures below 800 K. The optimum operating temperatures seem to be related to the thermal stability of the carbonates derived from the oxides. In particular, CuO-$BaTiO_3$ is the most sensitive to CO_2 among the oxides examined.

The effect of composition upon sensitivity to 2% CO_2 of the system $(CuO)_x(BaTiO_3)_{1-x}$ was further studied [47,48]. Exposure to 2% CO_2 slightly decreased the capacitance of the device below $x = 0.3$, but increased above $x = 0.3$. On the other hand, capacitance in air is too large to measure above $x = 0.7$. With increasing x, sensitivity to 2% CO_2 increased, and attained a maximum at the equimolar composition. Thus the equimolar composition, $(CuO)_{0.5}(BaTiO_3)_{0.5}$, is optimum for CO_2 detection. In spite of the chemical stability of carbon dioxide, these mixed oxide capacitors exhibit high selectivity for CO_2 detection as shown in Fig. 12. CH_4 and H_2, which are more reactive than carbon dioxide, had no appreciable effect on the capacitance. On the other hand, CO and H_2O did affect the capacitance. However, capacitance changes induced by CO appear to be caused not by CO itself, but by CO_2 formed on the device as evidenced by the effluent gas containing a significant amount of carbon dioxide, since Ag is active for CO oxidation [49]. On the other hand, adsorption of H_2O on the element increased the capacitance because of its large dielectric constant. However, the striking aspect of these sensors is that the capacitance change caused by CO_2 is larger than that by humidity at the same concentration. The sensitivity to 0.5% CO_2 on a CuO-$BaTiO_3$ element is shown in Fig. 13 as a function of the percentage humidity. Although the capacitance of CuO-$BaTiO_3$ element increased slightly after changing the dry air to the wet air, it remained nearly independent of the percentage humidity in the wet air. This may suggest that the amount of adsorbed water is very small due to the high operating temperature of the element and almost independent of the concentration of humidity. As a result, humidity hardly effects CO_2 detection under a practical operating conditions.

The addition of noble metals to semiconductor type gas sensors are sometimes effective in enhancing the sensing characteristics [50], e.g. CuO-$BaTiO_3$ [51]. Although the optimum operating temperature for CO_2 detection shifted slightly to higher temperature and longer response time, the sensitivity to 2% CO_2 was enhanced by the addition of metals or metal oxides. Figure 14 shows a plot of natural logarithm of sensitivity versus that of CO_2 concentration at 673 K. The lower limit of CO_2 detection with CuO-$BaTiO_3$ is 100 ppm. However, it decreased to 50 ppm

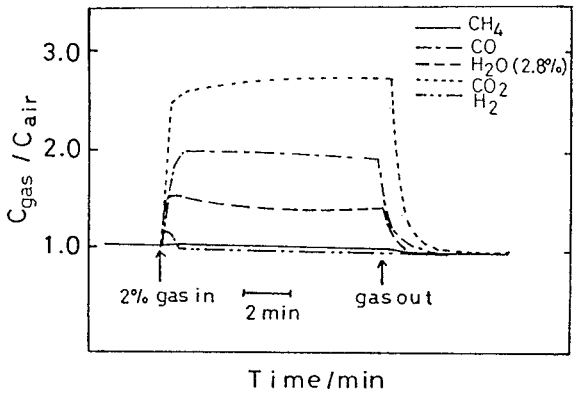

Fig. 12. Time dependence of capacitance of CuO-$BaTiO_3$ during the transient exposure to 2% CO_2, H_2, CH_4, CO_2, and 2.8% H_2O.

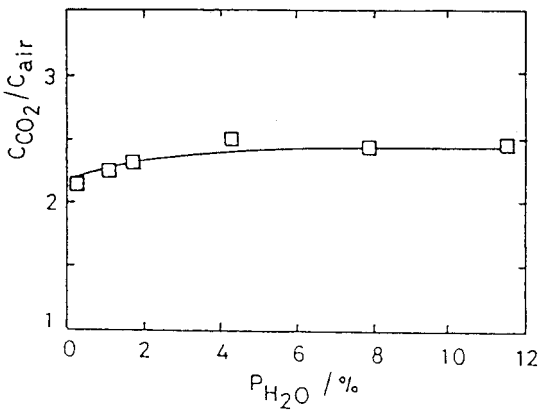

Fig. 13. Sensitivity of CuO-$BaTiO_3$ to 0.5% CO_2 as a function of humidity at an operating temperature of 729 K.

with the addition of Ag. Furthermore, the effects of Ag additions on the sensitivity were only observed on CO_2 sensitivity making CuO-$BaTiO_3$ even were selective for CO_2 as shown in Fig. 15. As a result, Ag added CuO-$BaTiO_3$ is effective for monitoring CO_2 concentrations in the atmosphere and it is those promising for practical applications.

The detection mechanism of these CuO-$BaTiO_3$ mixed oxide capacitors was investigated by complex impedance and I-V measurements [52]. Cole–Cole plots of the CuO-$BaTiO_3$ element consist of the three semicircles as shown in Fig. 16. The second semicircle appears only when CuO is mixed with $BaTiO_3$ and becomes more significant with increasing CuO content. The three semicircles were assigned to grain, grain boundary, and electrode interfaces. As shown in Fig. 16, exposure to CO_2 mainly changes the semicircle assigned to the grain junction between CuO and $BaTiO_3$. From seebeck coefficient measurements, CuO and $BaTiO_3$ are p- and n-type semiconductors, respectively, leading to the formation of potential barriers at the grain junctions between CuO and $BaTiO_3$. Since the CuO/$BaTiO_3$ junctions are randomly distributed in the element, rectification is not observed. However, in air, the element shows varistor-like non-linear I-V curves consistent with potential barriers existing at the grain junctions between CuO and $BaTiO_3$ as predicted. On the other hand, the I-V curves become ohmic in air containing 2% CO_2. The decrease in the height of the potential barrier leads to a narrowing depletion layer leading to an increase in capacitance.

Capacitive type NO_X sensors based on the same principle were also investigated [53,54]. Table 3 summarizes the sensitivity to 100 ppm NO over various mixed oxides. As expected, reproducible capacitance response to NO were exhibited on all elements examined. The capacitance of the mixed oxide generally decreased upon exposure to NO. Among the examined mixed oxides, it was found that a large capacitance increase was observed on CoO-In_2O_3 upon exposure to 100 ppm NO as shown in Table 3. It was reported that this CoO-In_2O_3 mixed oxide has high sensitivity to NO, but rather small

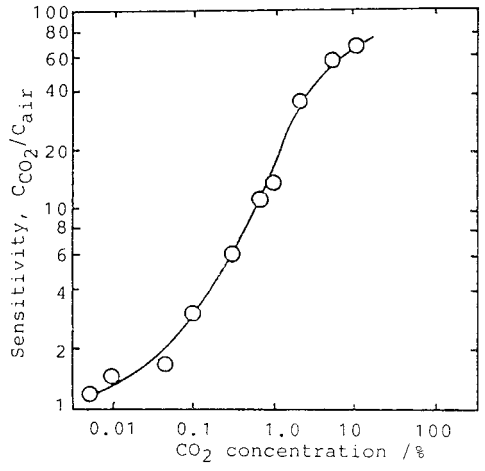

Fig. 14. Sensitivity of Ag added CuO-$BaTiO_3$ as a function of CO_2 concentration.

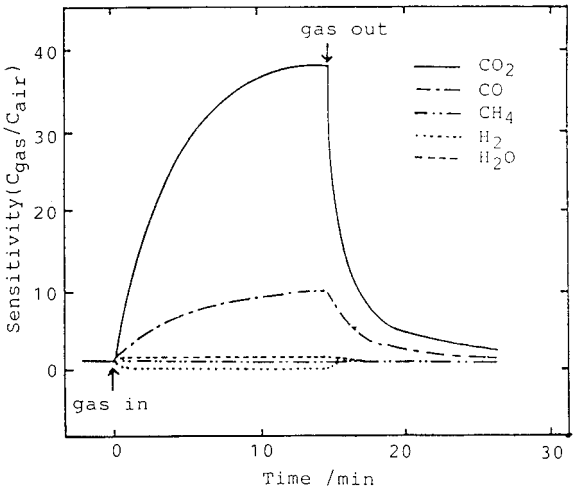

Fig. 15. Response of Ag added CuO-$BaTiO_3$ element after exposure to air containing 2% CO_2.

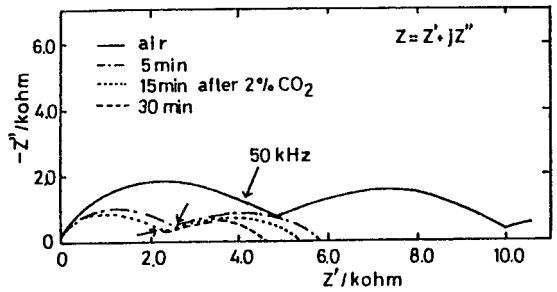

Fig. 16. Cole–Cole plots of $CuO\text{-}BaTiO_3$ against NO concentration in N_2 and in air.

sensitivity to CO, CO_2, SO_2, and H_2O, and clearly no sensitivity to NO_2 [54].

The capacitance of $CoO\text{-}In_2O_3$ becomes more sensitive to NO at low oxygen partial pressure. The sensitivity to NO in N_2 and air is shown in Fig. 17. The capacitance of the $CoO\text{-}In_2O_3$ mixed oxide increased linearly with increasing NO in the range from 0.1 to 100 ppm NO in N_2 but was almost insensitive to NO below 3 ppm in air. These results suggest that $CoO\text{-}In_2O_3$ is highly selective to NO, and the detection of NO in the range of a few 100 ppb level became feasible in an atmosphere without oxygen making it attractive as a NO sensor for flue gas analysis in internal combustion engines.

Mixed oxides are, therefore, useful and effective materials for the development of capacitive type gas sensors. Forming hetero junctions of p- and n-type semiconductors increased the number of sensing points. Consequently, sensitive and selective detection can be achieved.

5. Development of Commercial Capacitive Type Sensors for Monitoring CO_2

CO_2 sensors with high humidity-resistance and low-cost are required in the field of indoor air quality monitoring. Capacitive type CO_2 sensors consisting of $CeO_2/BaCO_3/CuO$ have been developed for this aim [55]. The principle of operation of this sensor is similar to that of the capacitive type sensor based on p-n junctions as described above. In this section, the capacitive type CO_2 sensor was reviewed from the viewpoint of practical application. Since sensor elements for monitoring indoor air quality are sometimes operated at high humidity, 40–90% RH, they must remain stable in such environments. while $CuO\text{-}BaTiO_3$ with small amounts of Ag exhibits high sensitivity, the capacitance gradually changes over several months. This may result from aggregation of the silver electrode. In addition, some amount of CO_2 is irreversibly adsorbed on $BaTiO_3$ resulting in changes in the carrier density. Mixtures of CeO_2-$BaCO_3$-CuO were selected given its enhanced

Table 3. NOx sensing characteristics of the examined binary mixed oxide

	Operating temperature[a] (°C)	Air level (nF)	Sensitivity C_{air}/C_{NO}[b]	90% response (s)	90% recover (min)
WO_3-ZnO	470	0.289	2.26	8	45
WO_3-CuO	381	1.738	2.08	15	35
WO_3-NiO	365	0.145	1.74	10	15
WO_3-SnO_2	176	0.144	7.74	210	55
WO_3-MgO	319	0.030	1.22	210	35
WO_3-Fe_2O_3	384	1.204	2.25	15	[c]
NiO-V_2O_3	170	158	1.74	180	[c]
NiO-$BaTiO_3$	509	0.077	0.68	360	25
NiO-$SrTiO_3$	–	–	1.00	–	–
NiO-ZnO	262	0.679	20.4	30	[c]
NiO-SnO_2	218	0.471	7.68	61	[c]
NiO-In_2O_3	261	250	0.32	85	11
NiO-$BaSnO_3$	–	–	1.00	–	–
ZnO-SnO_2	265	0.091	4.15	22	[c]
ZnO-In_2O_3	373	844	0.33	243	15
$CoO\text{-}In_2O_3$	129	0.040	0.06	193	[c]

[a] Temperature at the maximum sensitivity.
[b] Sensitivity to 100 ppm NO.
[c] Capacity did not restore to the air level within 60 min.

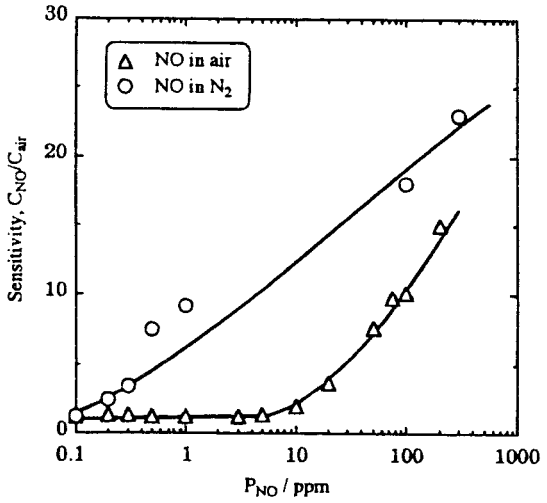

Fig. 17. Sensitivity to NO on $CoO\text{-}In_2O_3$ against NO concentration in N_2 and in air.

stability, albeit the sensitivity was decreased comparing that of CuO-BaTiO.

Figure 18 shows a schematic view of the developed sensor. Heater and electrodes are screen printed on Al_2O_3 plates $3.6 \times 2.8 \times 0.4$ mm. The ceramic plate consisting of CeO_2-$BaCO_3$-CuO (68:6:31) and dimensions $1.6 \times 1.2 \times 0.5$ mm is attached on to the Al_2O_3 plate with RuO_2 paste after sintering at 1173 K for 5 h. The sensor element is then fixed in the polymer container. Under operation, the sensor is heated to temperatures of 723–873 K. The power consumption is designed to be 0.7–1.3 W. The resulting sintered plate consisted of a uniform sized particle of diameter ca.0.3 μm. The relative density of the sensor element is estimated to be 0.7, providing enough porosity for gas permeation as well as adequate mechanical strength for handling. The X-ray diffraction pattern consisted of peaks from the starting phases of CeO_2, $BaCO_3$, CuO, and reacted phases of BaO and $BaCuO_2$ with peaks for the latter rather weak.

The capacitance of the element is decreased upon exposure to CO_2 and the sensitivity is expressed by the following equation,

$$S = [10 \times \log(C_{CO_2}/C_0)]$$

In this equation, C_0 represents the capacitance of the element in air containing 350 ppm CO_2. Although the capacitance of $BaCO_3$-CuO is unchanged upon exposure to CO_2, $BaCO_3$-CuO-CeO_2 exhibits a capacitance change and the sensitivity increases

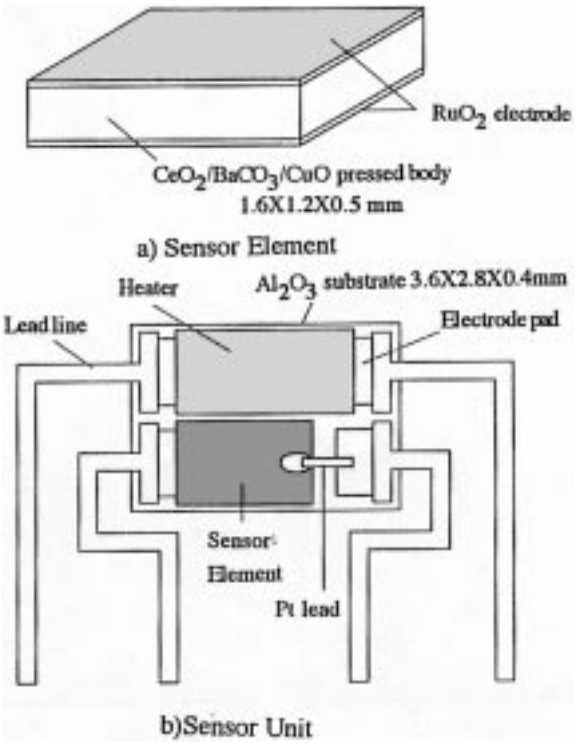

Fig. 18. Schematic view of the developed capacitive type of CO_2 sensor for monitoring indoor CO_2.

with increasing content of $BaCO_3$. A mixture of $BaCO_3$-CeO_2 also exhibits a capacitance change, albeit a far smaller change. Therefore, the CeO_2-$BaCO_3$ interface is the sensing part of this mixed oxide capacitor, with CuO serving as the sensitizer like in the CuO-$BaTiO_3$ type capacitive CO_2 sensors. The mixture CeO_2:$BaCO_2$:CuO = 63:6:31 gives the highest sensitivity with the sensitivity increasing with increasing temperature and attaining a maximum at 823 K. In addition, the highest sensitivity to 2% CO_2 is attained at a frequency of 50 kHz.

Figure 19 shows linear changes in sensitivity as a function of CO_2 concentration in the range from 350 ppm to 2%. The response and recovery times upon exposure to 2% CO_2 are nearly 3 min. Since the concentration of indoor CO_2 changes on the time scale of minutes, the response time is satisfactory. Figure 20 shows the durability of sensor sensitivity after keeping the element at 358 K and 90% RH with 2% CO_2 as the sensing gas. High sensitivity was sustained after 1500 h exposure with little degradation. This satisfies requirements for normal operation in 40–80%RH. and 273–300 K, respectively. Electrode materials also are

important with respect to stability. In case of Pt electrodes, the sensitivity to 2% CO_2 decreased to 90% of initial values after 350 days continuous operation. In contrast, sensors with RuO_2 electrodes exhibit a small increase in sensitivity in the initial 50 days and almost no degradation in the following 300 days. Therefore, RuO_2 is the electrode of choice. For commercialization of indoor CO_2 monitoring sensors, negligible degradation over 3 years is required. Durability tests of the mixed oxide capacitor with RuO_2 electrodes are still under measurement.

5.2. *Practical Monitoring Indoor CO_2 by the Developed Capacitive Type Sensor*

The developed capacitive type CO_2 sensor was combined with the signal treatment circuit and applied for monitoring indoor CO_2 concentration. For the signal treatment circuit of the commercial CO_2 sensor, simple, a cheap and reliable circuit is essential. Measurement of the capacitance is performed by the simple oscillator circuit with CMOS inverter as shown in Fig. 21. In this circuit, the capacitance of the element is converted into frequency (f) which is expressed by the following equation.

$$f = 1/(2.2 \times C \times R)$$

Here, C and R represent the capacitance of the sensor and standard resistance, respectively. Therefore, theoretically, the standard resistor and the frequency counter are only required for the signal treatment circuit. The simple signal treatment circuit is one of the great advantages of the capacitive type

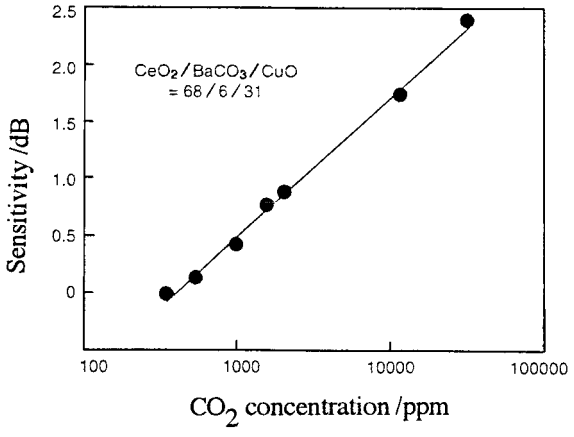

Fig. 19. Sensitivity of element as a function of CO_2 concentration.

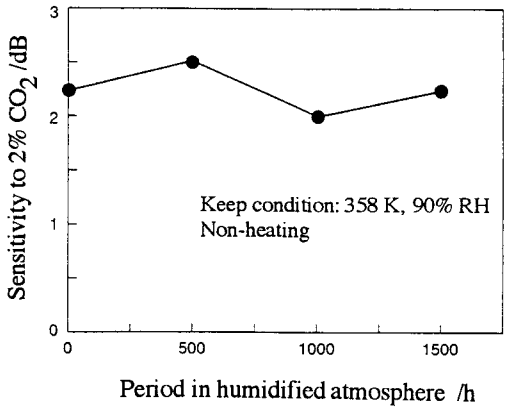

Fig. 20. Sensitivity of sensor element 2% CO_2 as a function of period kept at 358 K, 90% RH.

sensor. In the developed system, R is adjusted for the frequency in air to be 500 KHz and the CO_2 concentration was detected by the frequency shift from 500 kHz. The frequency shift was linearly increased with increasing CO_2 concentration from 350 to 2000 ppm as designed. Therefore, CO_2 concentration can be successively evaluated by shift in the frequency of an oscillator circuit. In addition, it was confirmed that the influence of water was negligible. On the other hand, a temperature change of the atmosphere caused the shift in frequency due to change in sensor temperature. Therefore, a thermistor was combined to remove the influence of temperature change. The sensor output for monitoring CO_2 concentration in an office room was shown in Fig. 22 as a function of time. In response to human activity, CO_2 concentration increased during the working period and decreased at night. An air conditioner was used continuously in the monitored

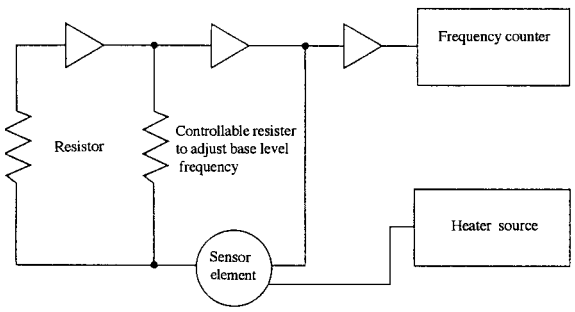

Fig. 21. Actuator circuit used for the developed capacitive type CO_2 sensor.

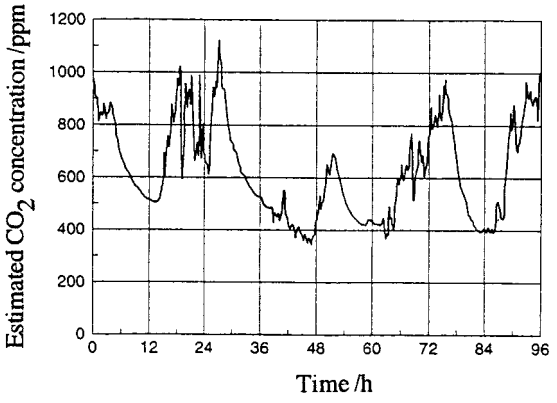

Fig. 22. Results of CO_2 monitoring in office of our research laboratory with developed system.

room and so, CO_2 concentration is decreased to 350 ppm, the normal air level, early in the morning. CO_2 concentration was simultaneously monitored with IR absorption type CO_2 meters and the estimated CO_2 concentration with both methods was always agreed within 5%. Therefore, it concluded that the CO_2 concentration can be successfully monitored by the developed capacitive type CO_2 sensor.

6. Future Work and Conclusions

While various types of sensors are being developed, a key area for advancement in sensor research is in the development of so-called smart sensors, fabricated on silicon chips with associated signal handling circuits. Along with the growth of integrated circuit (IC) technology, highly desirable miniaturized and integrated sensors are currently being developed. The principle advantage of the capacitive type of sensor is the simple structure of the element and the feasibility in signal treatment as discussed. Capacitive sensors lend themselves to miniaturization by IC processing. Furthermore, changes in capacitance are highly selective for specific physical phenomena. In addition, capacitance generally depends on temperature. Therefore, multi sensing of temperature and gas concentration is also expected by one sensor element. Capacitive type sensors are also very attractive for smart sensors from this point of view. Although the number of researches on the capacitive gas sensor is small and the kind of gases detected by this type is still restricted, the capacitive type of sensor has a potential for the development of the new intelligent sensor. The development of the capacitive sensor for the selective gas analysis will be doubtlessly be accelerated in the near future.

References

1. K. Takahata, in *Chemical Sensor Technology*, **Vol. 1**, edited T. Seiyama (Kodansha, Japan, 1988), p. 39.
2. K. Satake, A. Kobayashi, T. Inoue, T. Nakahara, and T. Takeuchi, *Proc. 3rd. Inter. Meet. on Chem. Sensors*, (Cleveland, 1990), p. 334.
3. T. Maekawa, J. Tamaki, N. Miura, and N. Yamazoe, *Chem. Lett.*, **1991**, 575 (1991).
4. M. Akiyama, J. Tamaki, N. Miura, and N. Yamazoe, *Chem. Lett.*, **1991**, 575 (1991).
5. T. Ishihara, K. Shiokawa, K. Eguchi, and H. Arai, *Chem. Lett.*, **1988**, 997 (1988).
6. T. Ishihara, K. Shiokawa, K. Eguchi, and H. Arai, *Sensors and Actuators*, **19**, 259 (1989).
7. N. Yamazoe and N. Miura, *Solid State Ionics*, **86–88**, 987 (1996).
8. T. Seiyama, N. Yamazoe, and H. Arai, *Sensors and Actuators*, **4**, 85 (1983).
9. N. Yamazoe and Y. Shimizu, *Sensors and Actuators*, **10**, 379 (1989).
10. B.M. Kulwicki, *J. Am. Ceram. Soc.*, **74**, 697 (1991).
11. M. Hijikigawa, H. Fukubayashi, S. Miyoshi, and Y. Inami, *Proc. 4th Sensor Symp.*, (Tsukuba, 1984), p. 135.
12. M. Hijikigawa, T. Sugihara, J. Tanaka, and M. Watanabe, *Proc. 2nd Solid-State Sensors and Actuators (Transducers'85)*, Philadelphia, p. 221.
13. S.V. Silverthorne, C.W. Watson, and R.D. Baxtor, *Sensors and Actuators*, **19**, 371 (1989).
14. K. Suzuki, K. Koyama, T. Inuzuka, and Y. Nabeta, *Proc. 3rd Sensor. Symp.*, (Tsukuba, 1983) p. 251.
15. V.K. Khanna and R.K. Nahar, *Sensors and Actuators*, **5**, 187 (1984).
16. Y. Sadaoka and Y. Sakai, *Proc. Inter. Meet. on Chem. Sensors*, (Fukuoka, 1983), p. 416.
17. M. Takeuchi, Y. Minamiya, F. Kaneko, and H. Nagasaki, *Proc. Inter. Meet. on Chem. Sensors*, (Fukuoka, 1983), p. 422.
18. Y. Nabeta, *Proc. Inter. Meet. on Chem. Sensors*, (Fukuoka, 1983), p. 410.
19. G.J. Rogers, L.C. Westcott, R.A. Davies, H.O. Ali, G.H. Swallow, and E. Read, *Proc. Inter. Meet. on Chem. Sensors*, (Fukuoka, 1983), p. 428.
20. W. Smetana and W. Wiedermann, *Sensors and Actuators*, **11**, 329 (1987).
21. H. Grange, C. Bieth, H. Boucher, and C. Delapierre, *Sensors and Actuators*, **12**, 291 (1987).
22. K.J. Balkus, L.J. Ball, B.E. Gnade, and J.M. Anthony, *Chem. Mater.*, **9**, 380 (1997).
23. T. Ishihara and Y. Takita, *Catalysis* (edited by J.J. Spivey), *Royal Chem. Soc.*, **12**, 21 (1996).

24. K. Alberti, J. Haas, C. Plog, and F. Fetting, *Catalysis Today*, **8**, 509 (1991).
25. F. Menil, C. Lucat, and H. Debeda, *sensors & Actuators*, **B24–25**, 415 (1995).
26. P. Bataillard, F. Gardies, N. Jaffrezic-Renault, and C. Martlet, *Anal. Chem*., **60**, 2374 (1988).
27. F. Gradies and C. Martelet, *Sensors and Actuators*, **17**, 461 (1989).
28. V. Billard, C. Martelet, P. Binder, and J. Therasse, *Analytica Chimica Acta*, **249**, 367 (1991).
29. U. Schoeneberg, B.J. Hosticka, G. Zimmer, and G.J. Maclay, *Sensoors & Actuators*, **B1**, 58 (1990).
30. F. Winquist, A. Spetz, M. Armgarth, and I. Lundstrom, *Sensors and Actuators*, **8**, 91 (1985).
31. S.V. Silverthorne, C.W. Watson, and R.D. Baxtor, *Sensord & Actuators*, **19**, 371 (1989).
32. W.P. Kang and C.K. Kim, *J. Electrochem. Soc*., **140**, L125 (1993).
33. M. Nagai and T. Nishio, *Sensors and Actuators*, **15**, 145 (1988).
34. Y. Ishiguro, Y. Nagawa, and H. Futata, *Proc. 2nd Inter. Meet. on Chem. Sensors*, (Bordeaux, 1986) p. 719.
35. T. Yoshioka, N. Mizuno, and M. Iwamoto, *Chem. Lett*., **1991**, 1249 (1991).
36. Y. Shimizu, K. Komori, and M. Egashira, *J. Electrochem. Soc*., **136**, 2256 (1989).
37. R. Cote, C.W. Bole, and M. Gautier, *J. Electrochem. Soc*., **131**, 63 (1984).
38. T. Maruyama, S. Sakai, and Y. Saito, *Solid State Ionics*, **23**, 107 (1987).
39. T. Ogata, S. Fujitsu, M. Miyayama, K. Koumoto, and Y. Yanagida, *J. Mater. Sci. Lett*., **5**, 285 (1986).
40. J. Liu and W. Weppner, *Solid State Commun*., **76**, 311 (1990).
41. S. Yao, Y. Shimizu, N. Miura, and N. Yamazoe, *Chem. Lett*., **1990**, 2033 (1990).
42. T. Ishihara, K. Kometani, M. Hashida, and Y. Takita, *Chem. Lett*., **1990**, 2033 (1990).
43. T. Ishihara, K. Kometani, M. Hashida, and Y. Takita, *Proc. 3rd Inter. Meet. on Chem. Sensors*, (Cleveland, 1990) p. 188.
44. T. Ishihara, K. Kometani, Y. Mizuhara, and Y. Takita, *J. Electrochem. Soc*., **139**, 2881 (1992).
45. T. Ishihara, K. Kometani, M. Hashida, and Y. Takita, *J. Electrochem. Soc*., **138**, 173 (1991).
46. T. Ishihara, K. Kometani, Y. Mizuhara, and Y. Takita, *Sensors and Actuators*, **B.5**, 97 (1991).
47. T. Ishihara, K. Kometani, Y. Mizuhara, and Y. Takita, *J. Am. Ceram. Soc*., **75**, 613 (1992).
48. T. Ishihara, K. Kometani, Y. Mizuhara, and Y. Takita, *Chem. Lett*., **1991**, 1711 (1991).
49. F.S. Stone, *Chemistry of Solid States* (Academic Press, New York, 1955), p. 367.
50. Y. Shimizu, Y. Fukuyama, T. Narikiyo, H. Arai, and T. Seiyama, *Chem. Lett*., **1985**, 377 (1985).
51. T. Ishihara, Y. Nishi, K. Kometani, Y. Mizuhara, and Y. Takita, *Chem. Let*., **1992**, 2297 (1992).
52. T. Ishihara, Y. Nishi, H. Nishiguchi, and Y. Takita, *Ceramic Sensors III* (edited by by Anderson, Liu, and Yamazoe), *Electrcochem. Soc*., **96–27**, p. 123.
53. T. Ishihara, S. Sato, and Y. Takita, *Sensors & Actruators*, **B24–25**, 392 (1995).
54. T. Ishihara, S. Sato, T. Fukushima, and Y. Takita, *J. Electrochem. Soc.,* **143**, 1908 (1996).
55. S. Matsubara, S. Shimizu, S. Kaneko, and S. Morimoto, *National Technical Report*, **43**(4), 15 (1997).